

IXPE Simulations for magnetars

Denis González-Caniulef¹ , Ilaria Caiazzo and Jeremy Heyl¹ 

¹Department of Physics and Astronomy, University of British Columbia,
Vancouver, BC V6T 1Z1, Canada

²TAPIR, Walter Burke Institute for Theoretical Physics, Mail Code 350-17, Caltech,
Pasadena, CA 91125, USA

Abstract. Due to the rich phenomenology and extreme magnetic conditions, magnetars will be targets of great interest for the upcoming polarimetry space missions. In particular, the Imaging X-ray Polarimetry Explorer (IXPE), recently launched in December 2021, will operate in the 2–8 keV range. This will open a new window to study the polarized, persistent X-ray emission from magnetars. In this talk, I will present simulations of IXPE observations of magnetars using the IXPEObsSim package. I will discuss future prospect to discriminate between different magnetar’s emission mechanisms, as well as a potential detection of the signal of vacuum birefringence using IXPE.

Keywords. stars: magnetars, polarization, scattering, stars: individual: 4U 0142+61

1. Introduction

Magnetars are neutron stars harboring strong magnetic fields, up to $B \sim 10^{14}$ G, which are thought to be main energy source for their bursting activity and X-ray luminosities. However, the emission mechanisms powering different parts of the spectra of magnetars remains unknown. The strong magnetic fields present in these sources hints that their X-ray emission should be substantially polarized. New X-ray polarimetry missions will open a new window to study magnetars, which will help us to understand the properties of matter and vacuum, as well as the transport of radiation, under strong magnetic fields.

Recently, the IXPE mission (Imaging X-ray Polarimetry Explorer) was successfully launched on December 2021. This soft X-ray polarimetry telescope will operate in the 2–12 keV range, for around 2 years (Weisskopf *et al.* 2016) and will observe a variety of X-ray sources. For magnetars, the observations are planned to start with 4U 0142+61, followed by 1RXS J170849.0-400910. The persistent soft X-ray spectrum of these sources is typically described by either a blackbody plus a power law (PL) or a double blackbody, which are generally interpreted as thermal emission from the surface plus non-thermal emission from the magnetosphere. In addition, they typically show a rising hard X-ray PL extending from ~ 10 keV up to ~ 100 keV.

In Caiazzo *et al.* (2021), we recently modeled the overall soft/hard X-ray spectrum and polarization of 4U 0142+61 considering different emission mechanisms. At the surface of the magnetar, we model the thermal emission from a gaseous atmosphere or a condensed surface, accounting for a varying surface thermal map and magnetic field. We also modelled soft X-ray emission from either hot spots or comptonization by hot electrons on the top of the atmosphere. In the magnetosphere, we consider reprocessing of the radiation by resonant cyclotron scattering (RCS) by charged particles moving in a twisted magnetosphere. In order to model the propagation of polarized radiation, we also account for vacuum birefringence induced by the strong magnetic field. The models

give a fairly good description of the X-ray emission of 4U 0142+61, and they produce unique polarization patterns in the IXPE band, which are discussed in the next sections.

2. Overview

Fig. 1 shows the spectrum and polarization of 4U 0142+61 (in the soft and hard X-ray bands), considering different mechanisms. We briefly summarize them below (for more details see [Caiazzo et al. 2021](#)).

Atmospheric emission. The thermal emission from NSs is expected to be reprocessed by an atmosphere. In a strong magnetic field, radiation propagates in the so-called O-mode and X-mode, which refer to electromagnetic waves with the electric field oscillating either parallel or perpendicular to the plane formed by the propagation direction and the magnetic field, respectively. In a magnetized plasma, the opacities in the X-mode are strongly suppressed compared to the O-mode. Therefore, the radiation becomes highly polarized in the X-mode, with polarization degree $PD \sim 99\%$. The transport of radiation in the atmosphere is solved numerically using Lloyd's code ([Lloyd 2003](#)), considering a fully ionized, hydrogen plasma.

Condensed surface. A strong magnetic field may drive a phase transition, turning a gaseous atmosphere into a condensed surface. The properties of the thermal radiation depend, particularly, on the composition and the highly unknown dielectric properties of the condensed surface. We consider an iron surface, which has more chances of being in a condensed state for typical temperatures and magnetic fields of magnetars. The dielectric tensor is assumed in the limit of free ions, meaning that ions fully respond to electromagnetic waves as Coulomb forces between them are relatively weak. The emissivity of the condensed surface is computed using the analytical expressions from [Potekhin et al. \(2012\)](#), and multiplied by the blackbody function to obtain the emergent spectrum. For a condensed surface the polarization is typically $PD < 20\%$, substantially lower than the atmospheric case (see e.g., [González Caniulef et al. 2016](#), [Taverna et al. 2020](#)).

Comptonization by hot electrons. We also consider a hot layer on the top of the atmosphere. Due to the strong field, the atmospheric O-mode photons are fully Comptonized by the hot electrons, while the X-mode photons freely escape. The output soft O-mode photons follow a fan beam (\sin^2) angular distribution. The resulting atmospheric emission plus O-mode Comptonized emission can give a good description of the whole soft X-ray spectrum of magnetars. In terms of polarization, a mode switch from X-mode to O-mode polarized radiation is present at energies in which full O-mode Comptonization starts to dominate over the atmospheric emission ($E \sim 5$ keV). On the other hand, the case of a condensed surface emission with a hot layer requires to model partial Comptonization, which has been left for a future work but it is expected to produce a polarization pattern similar to full O-mode Comptonization.

Thermal map & hot spots. Magnetars are expected to have a varying surface temperature as a result of the varying crustal conductivity (induced by the non-uniform magnetic topology). We model the thermal emission from the whole surface of the magnetar assuming that the temperature across the surface is determined by the direction of the local magnetic field with respect to the normal to the surface. As a first approach, we assume that the temperature map follows a dipolar field (thermal maps that account for the pulse profile are left for a future work). In such a case, the whole surface map is determined by fixing the temperature at the magnetic pole. We also include a hot spot at each magnetic pole with temperature and area that allow us to describe the whole soft X-ray emission from the magnetar. We consider atmospheric emission from the whole surface plus small atmospheric hot spots. Alternatively, we consider the scenario in which most of the surface is in a condensed state, with hot spots either in a condensed or atmospheric state.

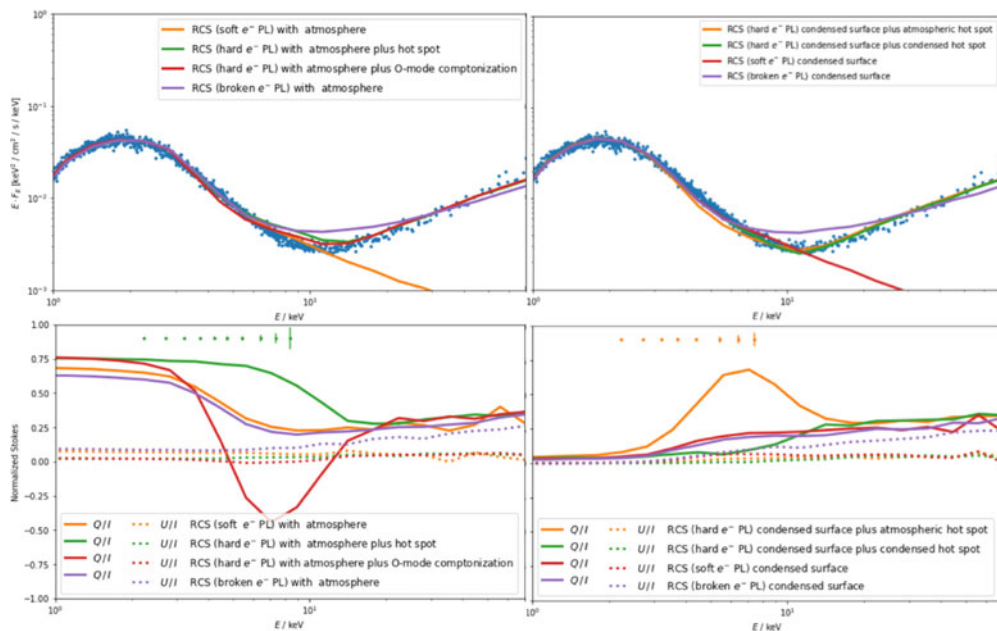


Figure 1. Spectrum (upper panels) and polarization (lower panels) for 4U 0142+61. Curves with different colors correspond to different surface models and RCS with different PL momentum distributions (for more details see Caiazzo *et al.* 2021). Panels on the left hand side correspond to atmospheric surface emission, while the panels on the right hand side show the case of condensed surface emission. All curves correspond to phase-averaged calculations for an orthogonal rotator. Blue points correspond to the unfolded spectrum taken from Tendulkar *et al.* (2015). In the lower panels, the green and orange error bars show the uncertainties in the Stokes parameters simulated for 1 Ms observations with IXPEObsSim. The green error bars correspond to the atmosphere plus hot spots model, and the orange error bars correspond to the condensed surface plus atmospheric hot spots.

Vacuum birefringence. A strong magnetic field induces the formation of virtual electron positron pairs, which modify the dielectric and magnetic permeability tensors of the vacuum. In magnetars, the X- and O-mode readapt to the local magnetic field as radiation propagates through the magnetosphere. The main effect of vacuum birefringence is that the polarization of the radiation reflects the magnetic field topology far from the NS surface, where the magnetic field across the plane perpendicular to the line-of-sight is nearly uniform. This produces a large polarization in comparison with that expected at the surface of the magnetar, where the non-uniform structures of the magnetic field reduce the polarization (Heyl & Shaviv 2000).

Resonant Cyclotron scattering. Magnetars are expected to have a twisted magnetosphere sustaining large currents of charged particles, which can create a substantial optical depth for X-ray photons. For typical magnetic fields of $B \sim 10^{14}$ G, RCS is effective at large distances, ~ 10 NS radii, where the field is relatively weak and the cyclotron energy of magnetospheric particles becomes comparable to the typical keV energy of the surface thermal photons (resonance condition). We model a magnetar with a twisted dipolar field, whose magnetospheric current is determined by the magnitude of the twist. In addition, we consider the particle flow with a PL momentum distribution, characterized by the PL index as well as the minimum and maximum Lorentz factors of the electrons (at variance with a Boltzmann momentum distribution that requires to specify the temperature of the particles). Alternatively, we also consider a broken PL momentum distribution further specified by an additional Lorentz factor parameter that sets the

slope break. This enable us to give a fairly good description of the hard X-ray emission or (partially) the whole soft and hard X-ray emission from the magnetar. To model the RCS process, we use the code discussed in Fernández & Davis (2011), which has been expanded to include thermal radiation from either an atmospheric or condensed surface. In terms of polarization, for the region of the spectrum in which RCS dominates, the polarization is typically $PD \sim 30\%$.

3. IXPE simulations and discussion

Fig. 1, lower panels, shows the polarization pattern for different processes in the Stokes parameter space. All cases take into account for vacuum birefringence in the magnetosphere. In particular, for atmospheric emission plus hot spot emission, the expected polarization degree is larger than $PD \sim 80\%$ over the whole IXPE band (2 – 8 keV). On the other hand, atmospheric emission plus Comptonization by a population of hot electrons produce a clear trend in which the polarization pattern switch from X-mode to O-mode dominated radiation (around ~ 5 keV). In the case of atmospheric emission plus RCS, the polarization degree decreases from $PD \sim 80\%$ to nearly $PD \sim 60\%$ in the IXPE band. If we repeat a similar analysis but for a condensed surface emission, the expected polarization is in general lower than $PD \sim 25\%$. However, an interesting scenario is for a condensed surface with an atmospheric hot spot, for which the polarization pattern increases from nearly $PD \sim 10\%$ to $PD \sim 80\%$ in the IXPE band.

We perform simulations of 1 Ms observations of 4U 0142+61 using the IXPEObsSim package (Pesce-Rollins *et al.* 2019). The error bars for the Stokes parameters are shown in Fig. 1, lower panel. They correspond to two representative cases: i) atmospheric emission plus hot spots, considering 10 energy bins in energy, and ii) condensed surface emission plus atmospheric hot spots, with 8 energy bins in energy. Both cases show that the error bars for the Stokes parameters are sufficiently small, so 1 Ms observation with IXPE will allow us to discriminate between different emission mechanism.

The analysis presented above demonstrates that the IXPE mission will be fantastic to study the emission mechanisms and transport of radiation in magnetars. This sum up to a potential detection of vacuum birefringence, which has been highly discussed in the literature.

Acknowledgements: This work was supported by the Natural Sciences and Engineering Research Council of Canada (NSERC), [funding reference #CITA 490888-16]

References

- Caiazzo, I., González-Caniulef, D., Heyl, J., *et al.* 2021, arXiv:2112.03401
 Weisskopf, M. C., Ramsey, B., O’Dell, S., *et al.* 2016, SPIE, 9905, 990517.
 Tendulkar, S. P., Hascöet, R., Yang, C., *et al.* 2015, *ApJ*, 808, 32.
 Lloyd, D. A. 2003, astro-ph/0303561
 Potekhin, A. Y., Suleimanov, V. F., van Adelsberg, M., *et al.* 2012, *A&A*, 546, A121.
 Heyl, J. S. & Shaviv, N. J. 2000, *MNRAS*, 311, 555.
 Fernández, R. & Davis, S. W. 2011, *ApJ*, 730, 131.
 González Caniulef, D., Zane, S., Taverna, R., *et al.* 2016, *MNRAS*, 459, 3585.
 Taverna, R., Turolla, R., Suleimanov, V., *et al.* 2020, *MNRAS*, 492, 5057.
 Pesce-Rollins M., Lalla N. D., Omodei N., Baldini L., 2019, NIMPA, 936, 224.